

An Investigation of the Fracture and Fatigue Crack Growth Behavior of Forged Damage-Tolerant Niobium Aluminide Intermetallics

F. YE, C. MERCER, and W.O. SOBOYEJO

The results of a recent study of the effects of ternary alloying with Ti on the fatigue and fracture behavior of a new class of forged damage-tolerant niobium aluminide ($\text{Nb}_3\text{Al}-x\text{Ti}$) intermetallics are presented in this article. The alloys studied have the following nominal compositions: Nb-15Al-10Ti (10Ti alloy), Nb-15Al-25Ti (25Ti alloy), and Nb-15Al-40Ti (40Ti alloy). All compositions are quoted in atomic percentages unless stated otherwise. The 10Ti and 25Ti alloys exhibit fracture toughness levels between 10 and 20 MPa $\sqrt{\text{m}}$ at room temperature. Fracture in these alloys occurs by brittle cleavage fracture modes. In contrast, a ductile dimpled fracture mode is observed at room-temperature for the alloy containing 40 at. pct Ti. The 40Ti alloy also exhibits exceptional combinations of room-temperature strength (695 to 904 MPa), ductility (4 to 30 pct), fracture toughness (40 to 100 MPa $\sqrt{\text{m}}$), and fatigue crack growth resistance (comparable to Ti-6Al-4V, monolithic Nb, and inconel 718). The implications of the results are discussed for potential structural applications of the 40Ti alloy in the intermediate-temperature (~ 700 °C to 750 °C) regime.

I. INTRODUCTION

INTERMETALLIC compounds are being considered for possible high-temperature applications in advanced propulsion and energy systems.^[1–7] However, the structural applications of most intermetallics are limited by their limited ductility and damage tolerance. Like most intermetallic compounds, Nb_3Al , which has the A15 crystal structure^[7,8] (Figure 1(a)), has poor room-temperature ductility and limited damage tolerance. However, recent work^[1] has shown that the addition of Ti to Nb_3Al can stabilize a more favorable B2 crystal structure (Figure 1(b)), which has the five independent slip systems required for homogeneous plastic deformation.^[7–10]

In the cast condition, the resulting alloys have room-temperature ductilities of ~4 to 30 pct.^[1] The room-temperature fracture toughness levels in the cast and forged Nb-15Al-40Ti alloys may also range between ~40 to 100 MPa $\sqrt{\text{m}}$.^[2,3] Similar fracture toughness improvements have also been observed in Nb-Ti-Cr alloys containing ~37Ti.^[4,5] The fracture toughness improvements in the alloys containing 37 to 40 at. pct Ti are due largely to the very significant levels of crack-tip plasticity in the alloy.^[6] The tough Nb-15Al-40Ti alloy also has a moderate density of ~6.08 g/cm³, which is in between that of titanium alloys and superalloys.^[1]

In this study, the effects of alloying Nb_3Al with Ti were examined in three different forged alloys (10Ti, 25Ti, and 40Ti). The fatigue and fracture behavior of all the alloys were examined at room temperature. The transition from relatively low fracture toughness levels (10 to 20 MPa $\sqrt{\text{m}}$) in the 10Ti and 25Ti alloys to high fracture toughness lev-

els (40 to 110 MPa $\sqrt{\text{m}}$) in the 40Ti alloy is associated with the onset of significant levels of crack-tip plasticity. Fatigue crack growth was also studied in the Nb-15Al-40Ti alloy at 750 °C (the potential oxidation temperature limit for uncoated niobium aluminide alloys is ~750 °C) in laboratory air. Slower near-threshold fatigue crack growth rates at an elevated temperature (750 °C) are shown to be due partly to the effects of oxide-induced crack closure.

II. MATERIAL

A. Processing and Microstructure

The alloys that were examined in this study were produced by Teledyne Wah Chang (Albany, OR). Nominal and actual ingot compositions are listed in Table I. Triple-melted ingots were produced by vacuum arc casting in a 11.4-cm-diameter × 25.4-cm-high mold. Ingots of the 40Ti alloy were reduced to billet form by conventional upset-forging processes. However, the 10Ti and 25Ti alloys cracked during conventional forging. These alloys were, therefore, processed using isothermal forging at 1250 °C and a constant strain rate of 0.25 s⁻¹.

The resulting microstructures of the forged products are presented in Figures 2(a) through (d). The forged 10Ti and 25Ti have microstructures consisting of A15 precipitates in a matrix of B2. An orthorhombic phase was also detected in the 25Ti alloy after annealing at 750 °C for 25 hours. The orthorhombic phases in the 25Ti alloy were distributed into star-shaped clusters in the B2 matrix. However, the 40Ti alloy contained only B2 grains in the as-forged condition. The amounts of A15 and orthorhombic phases present in these alloys were quantified using computerized image analysis techniques. The results were shown in Table II. All the alloys were tested in the as-forged condition and after annealing at 750 °C for 25 hours (direct aging (DA)). The behavior of the 40Ti alloy was also examined after solution treatment at 1150 °C for 8 hours and aging at

F. YE and C. MERCER, Postdoctoral Research Fellows, and W.O. SOBOYEJO, Associate Professor, are with the Department of Materials Science and Engineering, The Ohio State University, Columbus, OH 43210-1179.

Manuscript submitted October 24, 1997.

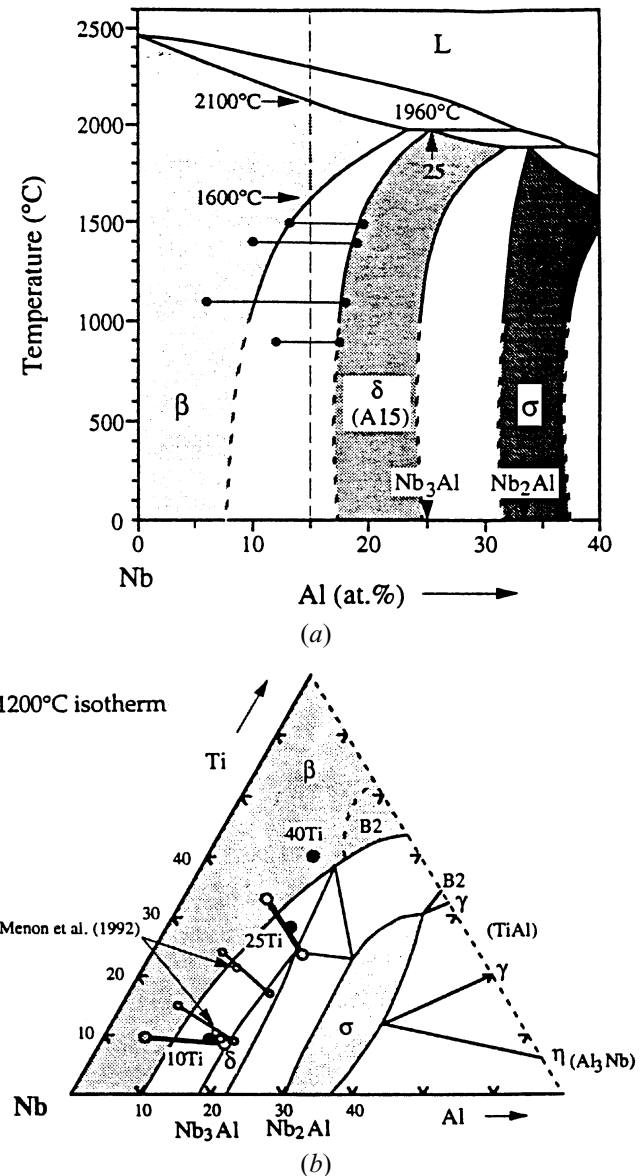


Fig. 1—(a) Binary Nb-Al phase diagram^[7] (b) 1200 °C isothermal section of ternary Nb-Al-Ti phase diagram.^[8,10]

750 °C for 25 hours (solution-treatment and aging (STA)). The 750 °C anneal was used to stabilize the microstructure at the potential oxidation temperature limit for the uncoated 40Ti alloy.^[10]

The as-forged microstructures of the 10Ti and 25Ti alloys consist of elongated B2 grains. The grains are elongated in the direction perpendicular to the forging direction (Figures 2(a) and (c)). Some needlelike orthorhombic grains were also identified in the 25Ti alloy. It is important to note here that the 10Ti and 25Ti alloys retained their elongated grain structure along with a small fraction of A15 precipitates following the 750 °C stabilization anneal (Figures 2(a) through (d)). However, the B2 structure of the 40Ti alloy was not fully retained after annealing at 750 °C for 25 hours (DA) followed by a furnace cool. This resulted in the formation of a two-phase microstructure, consisting predominantly of Widmanstätten orthorhombic platelets in a matrix of B2 (Table II).

Typical optical micrographs and transmission electron

micrographs of the heat-treated 40Ti alloy are presented in Figures 2(e) and (f), respectively. Unlike the 25Ti alloy (Figure 2(d)), the orthorhombic phase in the 40Ti alloy did not arrange itself into star-shaped clusters (Figure 2(f)). Instead, it forms predominantly Widmanstätten structures that completely fill the interior of the B2 grains. The structure and composition of the orthorhombic phase in the 25 and 40Ti alloy were similar to those reported in earlier studies of cast niobium aluminides.^[7] The chemical composition of the orthorhombic phase was Nb-25Al-43Ti, while the B2 phase had a composition of Nb-10Al-34Ti.^[7,8,9] The orthorhombic phase was formed in both the 25Ti and 40Ti alloys after annealing at 750 °C for 25 hours (Figures 2(c) through (f)). However, the as-forged 40Ti alloy had a purely B2 structure.

B. Tensile Properties

The tensile properties of the 10Ti, 25Ti, and 40Ti alloys are summarized in Table III. The results show that the 10Ti and 25Ti alloys exhibit limited ductility and low fracture stresses at room temperature. The 10Ti and 25Ti alloys also failed by brittle cleavage fracture modes in the as-forged and annealed conditions. However, the 40Ti alloy exhibits extensive ductility (~4 to 30 pct) and high yield strengths (695 to 904 MPa) at room temperature. The yield and ultimate tensile strengths of the 40Ti alloy also increase significantly upon annealing at 750 °C for 25 hours (DA). Furthermore, unlike most intermetallic materials, tensile fracture of the as-forged and annealed 40Ti alloy occurred by ductile dimpled fracture (Figure 3). Similar behavior has been observed in the cast 40Ti alloy.^[11]

The 40Ti alloy also exhibited strain softening behavior, and, hence, it does not have an ultimate tensile strength in the as-forged or heat-treated conditions. A typical stress-strain curve of the 40Ti alloy is shown in Figure 4. Note that the as-forged alloy exhibits a plastic strain to failure of ~30 pct at room temperature. However, the ductility of the 40Ti alloy decreases to ~4 pct after annealing at 750 °C for 25 hours (DA). Also, almost-zero ductility was observed after an 1150 °C/8 hours + 750 °C/25 hours (STA) treatment, which resulted in an intergranular fracture mode. A summary of room-temperature tensile properties of all the three alloys is presented in Table III.

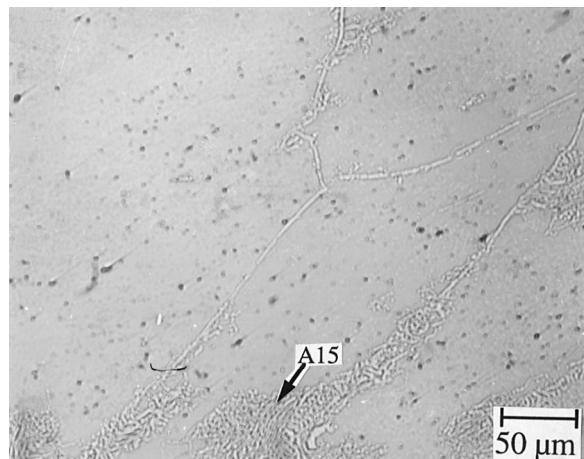
III. EXPERIMENTAL PROCEDURE

A. Fracture Toughness

Fracture toughness tests were performed on single-edge notched (SEN) bend-test samples (2.54 × 2.54 × 10.16 cm). The relatively large specimen dimensions were selected to promote plane strain conditions and to ensure that at least 50 grains (average grain size ~250 μm) were sampled by the through-thickness crack fronts during stable crack growth. The samples are precracked under far-field compression loading^[11] prior to fracture toughness testing under three-point bend loading. The fracture toughness test were performed in accordance with the ASTM E399 specifications.^[12] A loading rate corresponding to a stress intensity factor increase rate of 1 $\text{MPa}\sqrt{\text{m}\cdot\text{s}^{-1}}$ was used in the fracture toughness tests. The stress intensity factors were

Table I. Actual Compositions of Niobium Aluminide Alloys in Atomic Percent

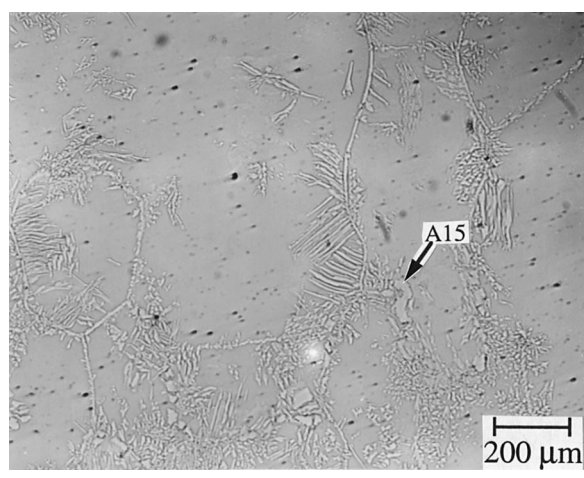
Alloy	Nb	Al	Ti	O	N	H	C	Cu
Nb-15Al-10Ti	bal	12.54	8.71	0.131	0.033	0.040	0.016	0.008
Nb-15Al-25Ti	bal	15.12	25.12	0.250	0.021	0.085	0.016	0.004
Nb-15Al-40Ti	bal	14.55	40.20	0.146	0.01	0.058	0.038	<0.01



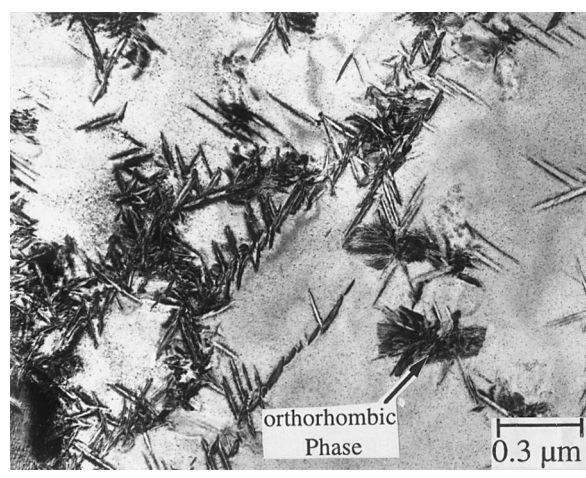
(a)



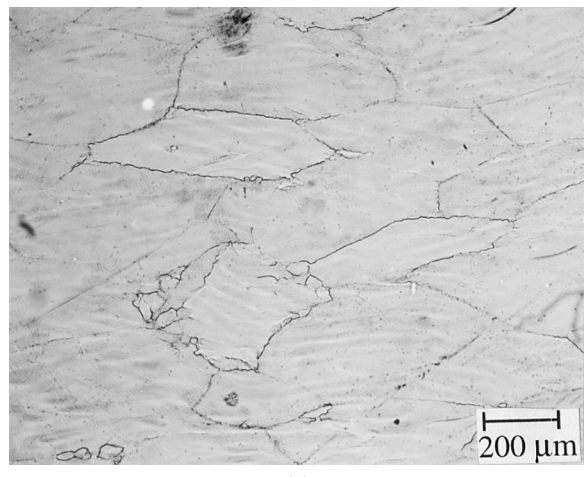
(b)



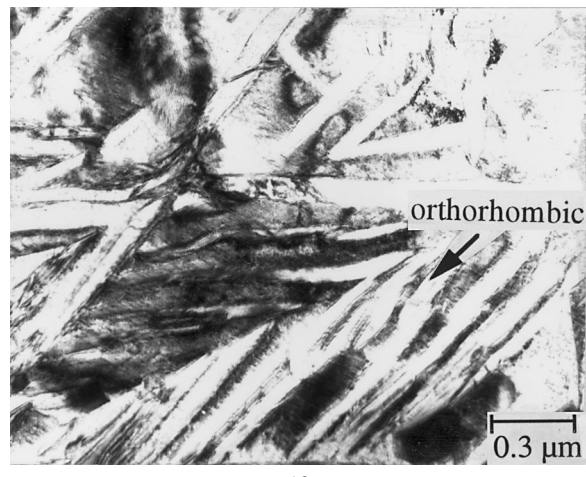
(c)



(d)



(e)



(f)

Fig. 2—Typical microstructure of forged (a) and (b) 10Ti, (c) and (d) 25Ti, and (e) and (f) 40Ti (750 °C/25 h). (a), (c), and (e) are optical micrographs, and (b), (d), and (f) are bright-field TEM micrographs.

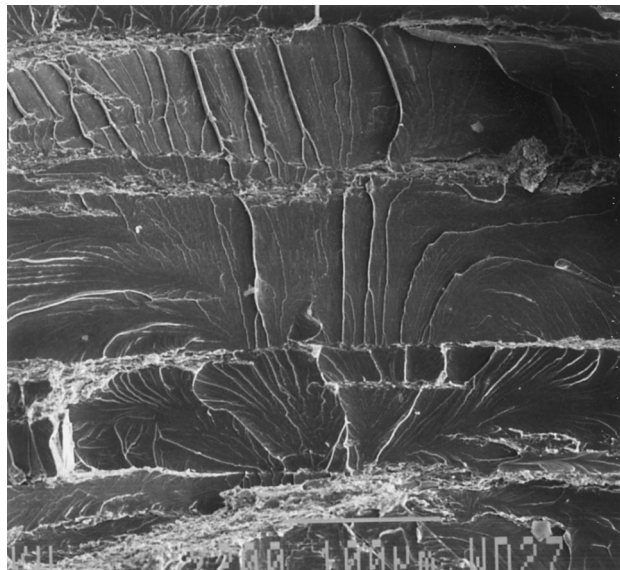
Table II. Volume Fraction of Phases Present in Niobium Aluminide Alloys

Phases	10Ti Alloy		25Ti Alloy		40Ti Alloy	
	As-Forged	DA	As-Forged	DA	As-Forged	DA
A15 Orthorhombic	7 ± 1.5 pct 0	7 ± 1.5 pct 1 ± 0.5 pct	9 ± 2 pct 0	9 ± 2 pct 18 ± 2.5 pct	0 0	0 85 ± 5 pct

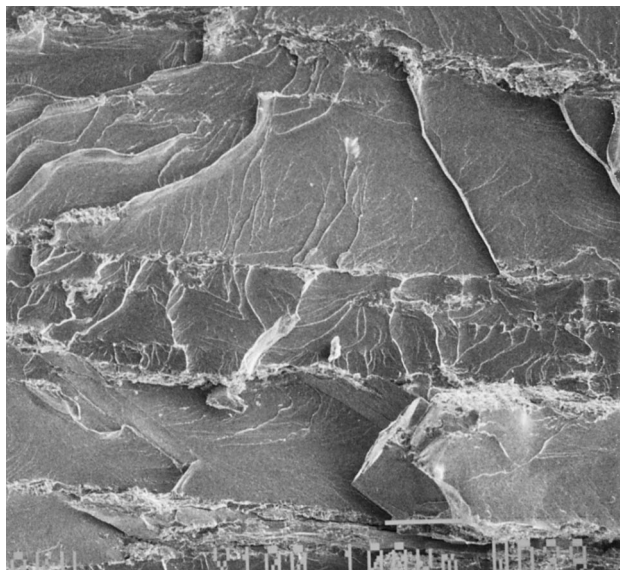
Table III. Room-Temperature Tensile Properties of Forged Nb-15Al-xTi Alloys

Tensile Property	10Ti		25Ti		40Ti	
	As-Forged	DA	As-Forged	DA	As-Forged	DA
Young's modulus E (GPa)	125 ± 3.0	77.4 ± 1.5	106 ± 1.5	71.4 ± 1.1	64.6 ± 0.7	101 ± 1.0
0.2 pct offset yield stress σ_y (MPa)	—*	—*	—*	—*	695 ± 18	904 ± 14
Ultimate tensile strength σ_{UTS} (MPa)	200 ± 19	98 ± 17	193 ± 21	377 ± 50	—	—
Total strain to failure ϵ_{Max} (pct)	0.17 ± 0.08	0.15 ± 0.07	0.19 ± 0.08	0.51 ± 0.1	29.5 ± 0.6	3.9 ± 0.9

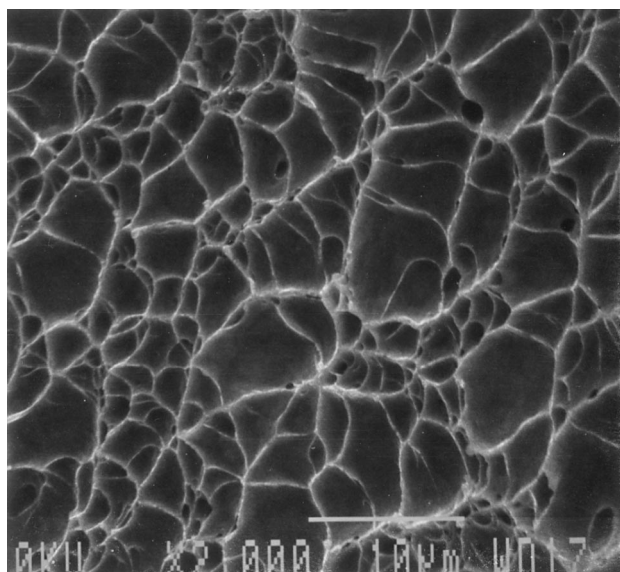
*Material fractured before yield.



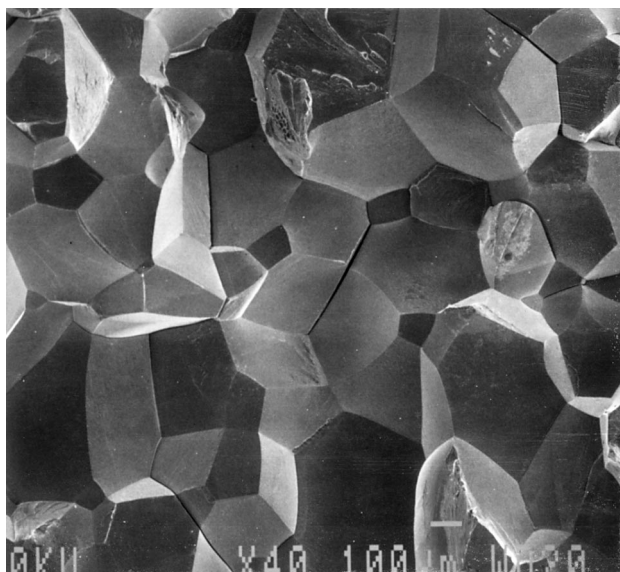
(a)



(b)



(c)



(d)

Fig. 3—Typical tensile fracture modes in (a) as-forged 10Ti, (b) as-forged 25Ti, (c) as-forged 40Ti, and (d) as-forged + 1150 °C/8 h + 750 °C/25 h heat-treated 40Ti.

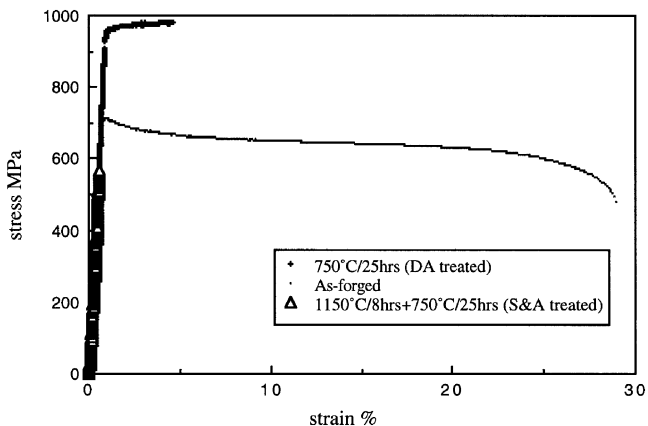


Fig. 4—Strain-stress curves obtained for Nb-15Al-40Ti alloy.

calculated using an expression provided in the ASTM E399 specifications.^[12]

B. Fatigue Crack Growth

Fatigue crack growth studies were carried out on 6.25-cm-long SEN bend specimens with square (25.4×25.4 mm) cross sections and lengths of ~ 10.16 cm. The initial notches were ~ 11 -mm deep. The SEN specimens were produced by electrodischarge machining techniques. All the fatigue crack growth experiments were carried out in a closed-loop servohydraulic testing machine. The SEN specimens were precracked in air using computer-controlled load-shedding techniques under three-point bend loading. A cyclic frequency of 10 Hz and a stress intensity factor range (ΔK) of ~ 20 to 25 MPa $\sqrt{\text{m}}$ were employed in the precracking. A load-shedding rate (C) of -0.08 (mm $^{-1}$) or -2 (inch $^{-1}$) was used in the fatigue crack growth testing, where C is given as.^[12]

$$K_{\max} = K_{\max 0} \exp [C(a - a_0)] \quad [1]$$

Note that K_{\max} is the current stress intensity; $K_{\max 0}$ is the initial stress corresponding to a_0 ; C is a constant with dimensions of 1/length, which is the controlling load shedding/increasing rate; a is the current crack length; and a_0 is the initial crack length.

After precracking, the fatigue crack growth experiments were also conducted under three-point bend loading at a cyclic frequency of 10 Hz. A stress ratio ($R = K_{\min}/K_{\max}$) of 0.1 was used. Fatigue crack growth was also monitored using a high-resolution ($2.5 \mu\text{m}$) telescope connected to a

video monitoring unit. This was used to verify the actual crack lengths during the tests. The fatigue thresholds were determined by load shedding. Note that the threshold was taken to correspond to a ΔK level at which no crack growth was detected after $\sim 10^7$ cycles. After testing, the polished sides of the specimens were examined under a scanning electron microscope. The interactions between the fatigue cracks and underlying microstructures were, thus, elucidated. The SEN specimens were then deformed continuously to failure under monotonic loading. Finally, the fracture surfaces of the specimens were studied under a scanning electron microscope.

IV. RESULTS

A. Fracture Toughness

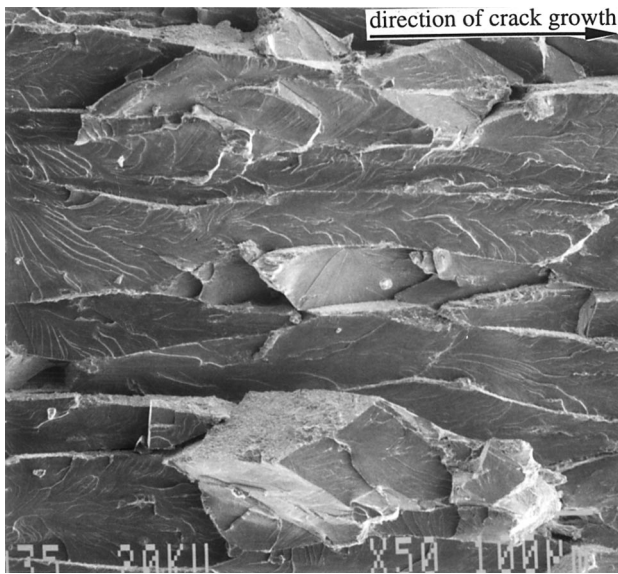
The fracture toughness data obtained from the forged alloys are summarized in Table IV. The fracture toughness increases from 10 to 20 MPa $\sqrt{\text{m}}$ in the 10Ti and 25Ti alloys to as high as about 100 to 110 MPa $\sqrt{\text{m}}$ in the 40Ti alloy. The latter values are some of the highest fracture toughness levels ever recorded for any ordered intermetallic alloy. The test conditions also generally satisfied the ASTM E-399 requirements. However, it is important to note that the specimen dimensions ($25.4 \times 25.4 \times 100$ mm) of the direct-aged 40Ti alloy did not fully satisfy all the ASTM E399 criteria. Nevertheless, the fracture toughness of 100 to 110 MPa $\sqrt{\text{m}}$ that was obtained in this condition was essentially independent of specimen thickness, for specimen thicknesses between 12.5 and 25.4 mm. The effects of thickness on fracture toughness, therefore, appear to be relatively small in this thickness regime.

Similar improvements in fracture toughness have also been obtained from a Nb-13Cr-37Ti alloy^[4,5] which has fracture toughness levels between ~ 65 to 85 MPa $\sqrt{\text{m}}$. As in the case of the 40Ti alloy, the improved fracture toughness in the Nb-13Cr-37Ti alloy was associated with the onset of significant levels of crack-tip plasticity. These will be discussed later. In any case, the 750 °C/25 hours (DA)-treated 10Ti and 25Ti alloys exhibit a significant increase in fracture toughness, from about 18 to 28 MPa $\sqrt{\text{m}}$. Fracture in the 10Ti and 25Ti alloys occurred by transgranular cleavage (Figures 5(a) through (d)). In contrast, the as-forged and DA-treated 40Ti alloys exhibit predominantly ductile dimpled fracture modes (Figures 6(a) and (b)). Ductile dimpled fracture was observed to occur in the forged 40Ti alloy along with secondary splitting along the grain boundaries of the forged direct-aged material (Figure 6(b)).

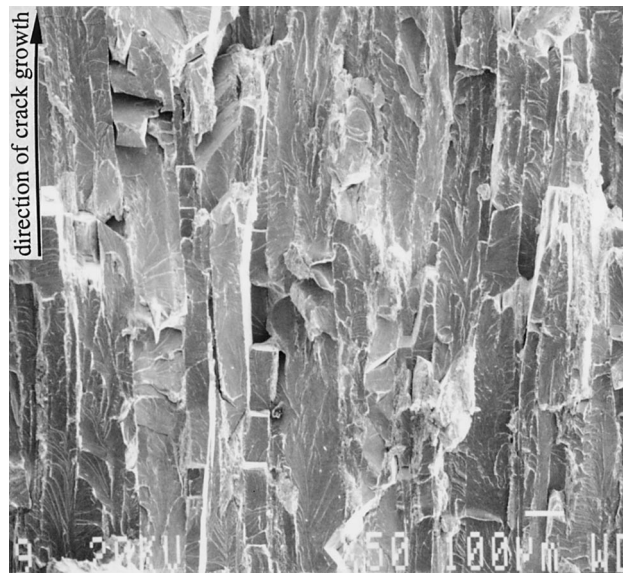
Table IV. Summary of Fracture Toughness Values and Fracture Modes

Material	Processing/ Heat Treatment	Phase(s)	Fracture Toughness (MPa $\sqrt{\text{m}}$)	Fracture Mode
Nb-15Al-10Ti	as-forged	B2 + A15	17 \pm 3	cleavage
	as-forged + 750 °C/25 h	B2 + A15	27 \pm 5	cleavage
Nb-15Al-25Ti	as-forged	B2 + A15	18 \pm 4	cleavage
	as-forged + 750 °C/25 h	B2 + A15 + O	29 \pm 5	cleavage
Nb-15Al-40Ti	as-forged	B2	110 \pm 10*	ductile dimpled
	as-forged + 750 °C/25 h	B2 + O	102 \pm 13*	ductile dimpled
	as-forged + 1150 °C/2 h + 750 °C/25 h	B2 + O	41 \pm 4	intergranular

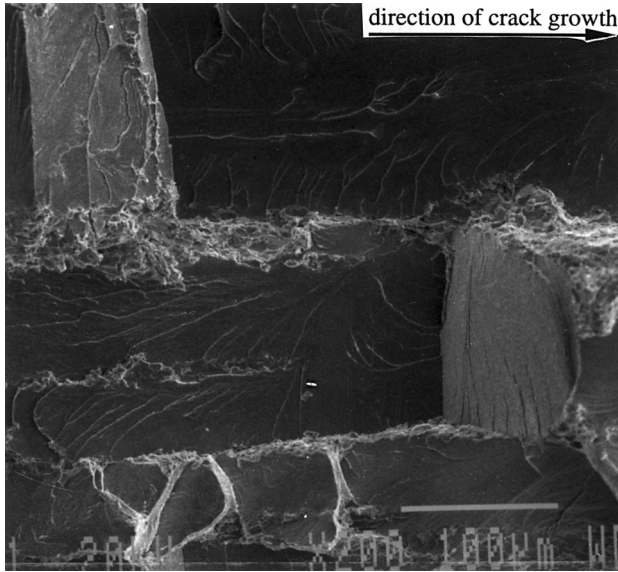
*Specimen did not fully satisfy ASTM E-399 specification for plane strain fracture toughness testing.



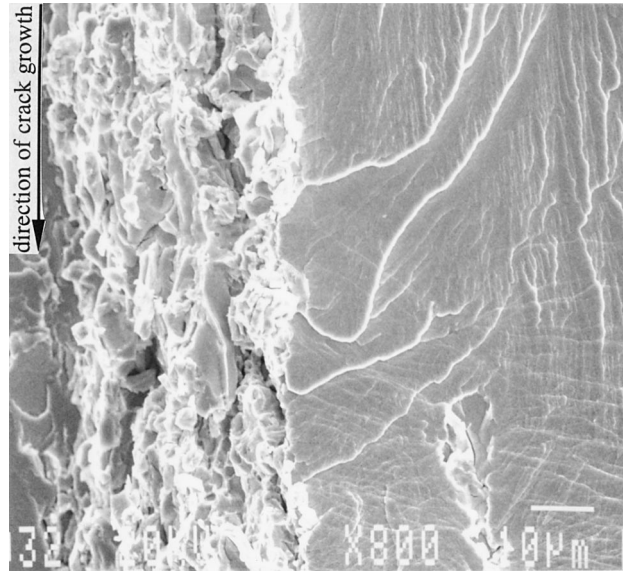
(a)



(b)



(c)



(d)

Fig. 5—Typical fracture modes in SEN fracture toughness specimens. Cleavage in forged 10Ti alloy: (a) as-forged and (b) as-forged + 750 °C/25 h; and cleavage in forged 25Ti alloy: (c) as-forged and (d) as-forged + 750 °C/25 h.

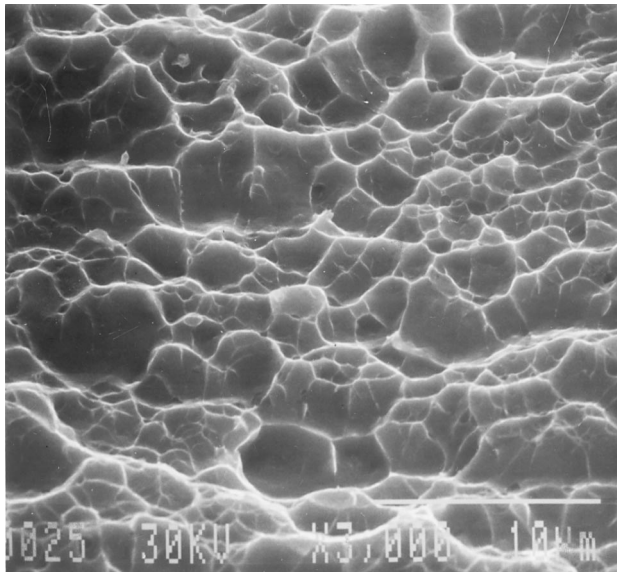
The STA heat treatment also resulted in a mixed fracture mode, consisting predominantly of intergranular facets (Figure 6(c)), with some incidence of ductile dimpled fracture (Figure 6(d)). However, unlike the 10Ti and 25Ti alloys, the occurrence of stable intergranular crack growth is associated with significantly lower fracture toughness levels in the solution-treated and aged 40Ti alloy tested in the 1150 °C/8 hours + 750 °C/25 hours (STA)-treated condition, which is about 40 MPa/m. Reasons for the lower fracture toughness after the STA treatment are unknown at present.

Nevertheless, it is important to note that evidence of significant levels of localized plasticity were observed in the deformed regions close to the fracture surfaces of the STA 40Ti alloy, as shown in Figure 7. Note that the slip bands in the regions close to the fracture surface are evidence of

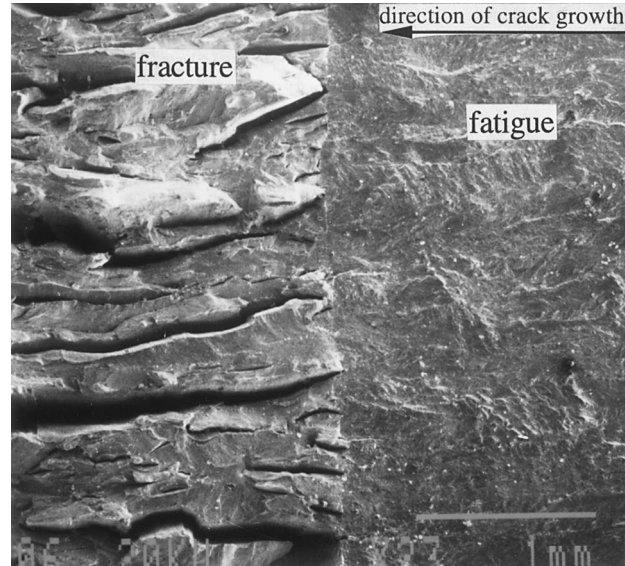
significant levels of localized plasticity before the onset of final intergranular failure. The occurrence of localized plasticity may, therefore, explain the relatively high toughness levels (compared to those of the 10Ti and 25Ti alloys) of ~40 MPa/m that were obtained in the STA condition, in spite of the incidence of intergranular failure. Finally, it is important to note that intergranular crack growth in the solution-treated 40Ti alloy may be due to the formation of submicron grain-boundary oxide precipitates, as suggested by Johnson^[13] in a recent Auger study of the 40Ti alloy.

B. Room-Temperature Fatigue Crack Growth and Thresholds

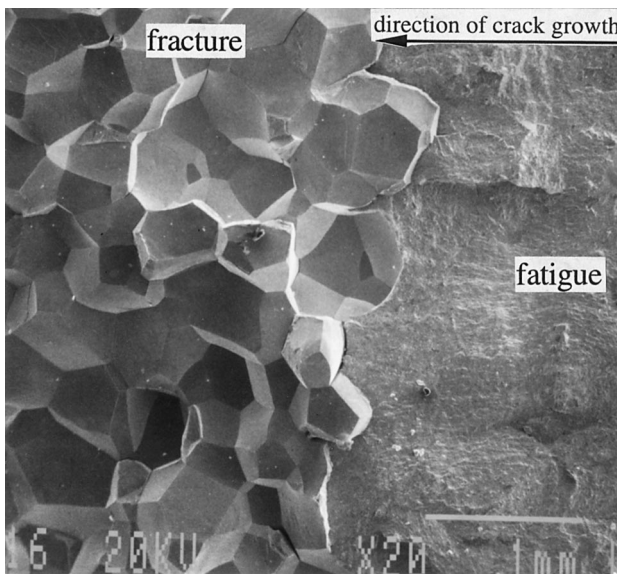
The room-temperature fatigue crack growth rates of the forged Nb-15Al- x Ti alloys are compared to those of forged



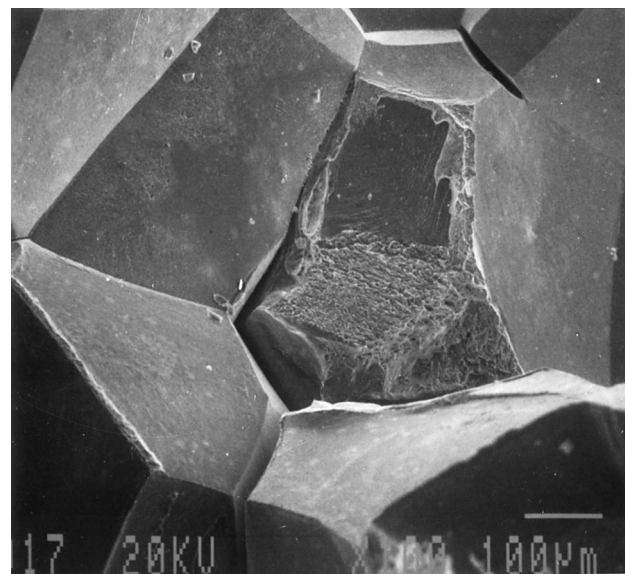
(a)



(b)



(c)



(d)

Fig. 6—Typical fracture modes in SEN fracture toughness specimens. Ductile dimpled fracture in forged 40Ti alloy: (a) as-forged and (b) as-forged + 750 °C/25 h; and (c) and (d) intergranular fracture in STA treated 40Ti alloy.

mill-annealed Ti-6Al-4V^[14] and IN718^[15] and pure Nb^[16] in Figures 8(a) and (b). The fatigue crack growth thresholds (ΔK_{th}) and Paris constants (A and m) are also summarized in Table V. The 10Ti and 25Ti alloys exhibit faster crack growth rates and higher Paris exponents than the 40Ti alloy. The fatigue crack growth rates in the 40Ti alloy are faster than those of IN718 in the as-forged condition. However, the crack growth rates in the 40Ti alloy are comparable to fatigue crack growth rates in mill-annealed Ti-6Al-4V. It is particularly important to note that the 40Ti alloy has Paris exponents between 2.2 and 4.4. These are close to the values of ~2 to 4 that are typically reported for ductile metals and their alloys.^[17]

The fatigue crack growth threshold levels in the as-forged 25Ti and 10Ti alloys (~6.4 and ~7.1 MPa $\sqrt{\text{m}}$, respectively) are greater than those of the 40Ti alloy (~5.1

MPa $\sqrt{\text{m}}$) in the as-forged condition. However, the fatigue crack growth rates in the 40Ti alloy are generally slower than those obtained for the 10Ti and 25Ti alloys in the Paris regime. The DA treatment also appears to have only a small effect on the fatigue crack growth behavior of the 10Ti and 25Ti alloys. However, the DA treatment has a significant effect on the 40Ti alloys, in which the fatigue threshold drops from ~8.6 to ~6.7 MPa $\sqrt{\text{m}}$ after DA treatment. The Paris exponents also decrease from 4.4 to 2.2 after DA treatment.

Inspection of the fracture surfaces of the fatigue samples reveals faceted cleavage fracture modes in the 10Ti and 25Ti alloys (Figures 9(a) and (b)). However, the DA-treated 40Ti alloy exhibits crystallographic fracture modes in the low- and mid- ΔK regimes and fatigue striations in the high- ΔK regime (Figures 10(a) and (b)). The lower Paris

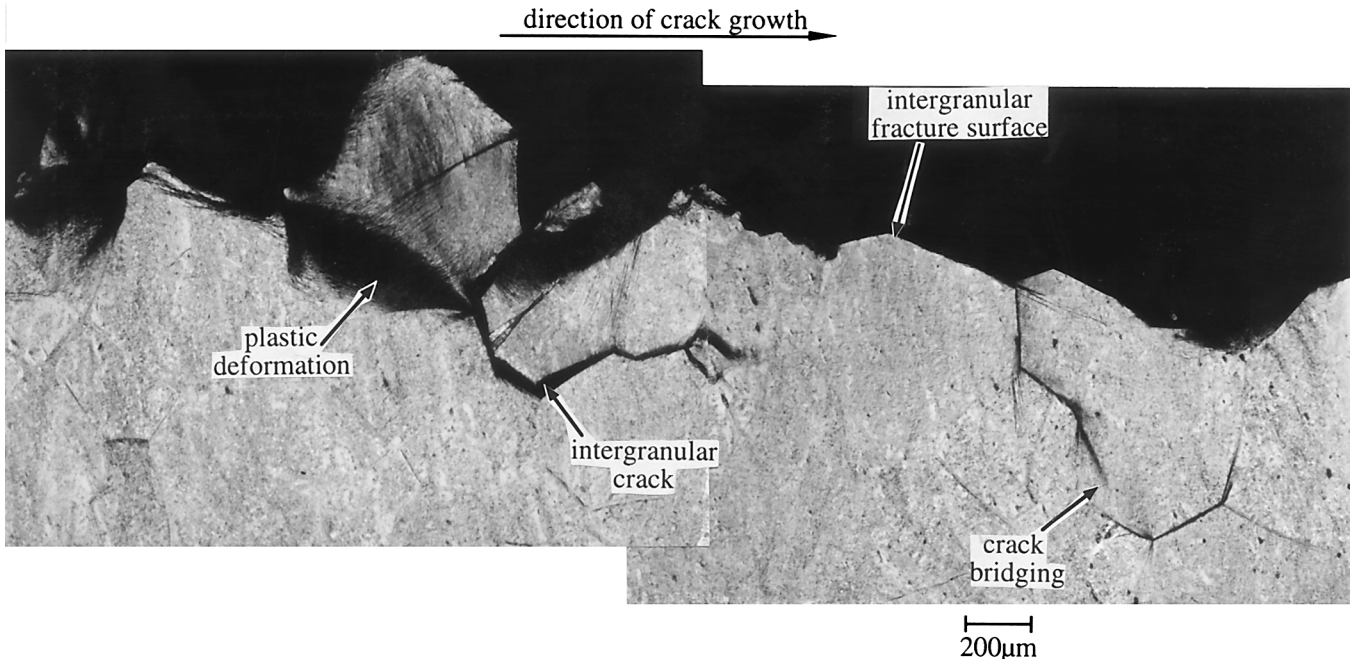


Fig. 7—Evidence of plasticity in STA treated 40Ti alloy.

exponents and slower fatigue crack growth rates in the 40Ti alloy were, therefore, associated with a transition from brittle to ductile crack growth mechanisms.

C. Elevated-Temperature Fatigue Crack Growth and Thresholds

The fatigue crack growth rate data obtained for the direct-aged, heat-treated 40Ti alloy at 750 °C in air are presented in Figure 11. The near-threshold crack growth rates obtained at 750 °C were slower than those obtained in air at 25 °C. Higher fatigue thresholds were also obtained at 750 °C (~8.2 MPa \sqrt{m}) compared to corresponding fatigue threshold values of ~5.1 MPa \sqrt{m} at 25 °C. The high elevated-temperature fatigue thresholds were associated with the presence of thick oxide layers that were observed on the fracture surfaces of the 40Ti specimens tested at 750 °C.

An X-ray analysis of these fracture surfaces was carried out on Scintag Pad-V X-ray diffractometer. The results (Figure 12) revealed that these fracture layers consisted predominantly of rutile (TiO_2). Evidence of fracture-surface oxidation was also obtained from the microstructural and fractographic examination of the crack profiles shown in Figures 13. These show clearly that oxide debris (Figure 13(a)) and an oxide layer (Figure 13(b)) are formed on the fracture surfaces of the fatigue specimens that were tested at 750 °C. Such oxide layers and debris can induce crack closure when the excess debris/oxide thicknesses are comparable to crack-tip opening displacements.

To explore this possibility, oxide-induced closure levels were estimated using a modified Dugdale–Barenblatt closure model.^[18] The model accounts for the wedging induced by an oxide layer that forms behind the crack tip. Since the composition and thickness of the oxide layer must be known in any detailed oxide-induced closure analysis, the

oxide layer on the fracture surfaces was characterized using X-ray spectroscopy and energy-dispersive X-ray spectroscopy. The oxide layer was shown to consist solely of TiO_2 . The excess oxide thicknesses and the wedge lengths of the oxide films were used in the estimation of the closure stress intensity factor (K_{cl}), which was estimated from the following expression due to Suresh and Ritchie:^[18]

$$K_{cl} = \frac{dE}{4(\pi l)^{1/2} (1 - \mu^2)} \quad [2]$$

where d is the excess oxide thickness, $2l$ is the wedge length of the oxide film, μ is the Poisson's ratio of ~0.3, and E is the Young's modulus of ~105 GPa. The excess oxide thickness was measured from the crack profiles of the 40Ti specimen. An average oxide of thickness of ~5 μm was measured in the 40Ti alloy following the threshold test. The wedge length was also measured at the end of the test. This was shown to be ~4.3 mm. With a Young's modulus of 105 GPa and a Poisson ratio assumed to be 0.3, the closure stress intensity level is, thus, estimated from Eq. 2 to be ~1.8 MPa \sqrt{m} at the threshold condition in the 40Ti alloy at 750 °C. Hence, the effective fatigue threshold ($\Delta K = \Delta K_{app} - \Delta K_{cl}$) was estimated to be ~6.6 MPa \sqrt{m} at 750 °C. This is close to the room-temperature fatigue threshold obtained for the 40Ti alloy at room temperature. This suggests that the differences between the fatigue thresholds and near-threshold crack growth rates at 25 °C and 750 °C are due partly to the effects of oxide-induced closure.

Consistent with the previous arguments, the fatigue crack growth rates in the mid- ΔK and high- ΔK regimes were comparable to those obtained at room temperature, where oxide-induced closure was not observed. This suggests that oxide-induced closure does not occur in mid- ΔK and high- ΔK regimes, where the crack opening displacements are much greater than the excess oxide thickness levels. The ineffectiveness of oxide-induced closure in this regime may

also be attributed partly to higher crack-tip opening displacements and the limited time available for fracture surface oxidation to occur in mid- and high- ΔK levels, where the fatigue crack growth rates are relatively fast.

V. DISCUSSION

A. Fracture Toughness

It is of interest to discuss the improvements in fracture toughness within the context of ongoing work on niobium-based intermetallics.^[19] First, it is important to note that the significant improvements in fracture toughness in the 40Ti alloy are associated with the onset of significant levels of crack-tip plasticity (Figure 7). This is consistent with the results of recent atomistic simulations of crack-tip plasticity by Farkas.^[19] Her analysis shows that dislocation emission is favored over cleavage as the Ti content is increased from 16 to 33 at. pct. Dislocation and crack-tip blunting were predicted by atomistic simulations of crack-tip deformation in {110} crystals oriented for crack growth in the ⟨100⟩ and ⟨111⟩ directions.

In contrast, the analysis of Farkas predicted that cleavage fracture was more likely to occur before dislocation emission occurred in an alloy containing lower amounts of Ti (16 pct). The onset of dislocation emission may, therefore, be considered as one of the reasons for the improved fracture toughness levels of the 40Ti alloy. However, further work is required to extend the atomistic simulations to the case of the 40Ti alloy. Modeling of Nb-15Al-40Ti polycrystals is also required, since the effects of polycrystalline constraint may limit the number of available slip systems. Nevertheless, the atomistic simulations of Farkas^[19] provide some valuable insights into the possible effects of alloying with Ti.

The measured fracture toughness levels of 40 to 110 MPa \sqrt{m} are clearly much higher than those reported previously for other intermetallic systems such as gamma-based titanium aluminides^[20] and MoSi₂.^[21] However, recent work on Nb-Cr-Ti alloys and *in-situ* composites^[4,5] has shown that significant improvements in fracture toughness (~65 to 80 MPa \sqrt{m}) can also be engineered in these bcc alloys by the addition of ~40 at. pct Ti. The beneficial effect of ~40 pct Ti was correlated with the lower number of d + s electrons per atom in the Nb-Cr-Ti system.^[4] In contrast, alloying elements that increase the number of d + s electrons per atom were shown to have lower ductilities. In any case, the Nb-Cr-Ti and Nb-Al-Ti alloys with ~40 at. pct Ti additions are of scientific and technological interest due to their high fracture toughness levels. These two alloy systems also appear to have the balance of properties required for structural applications at temperatures up to ~700 °C to 750 °C.

Finally, it is of interest to compare the measured fracture toughness levels to those reported by other workers for niobium-based alloys/intermetallics (Figure 14). The Laves phase (Nb-Cr-Ti) intermetallics and composites generally have fracture toughness levels between ~8 to 20 MPa \sqrt{m} at room temperature.^[22] However, the fracture toughness levels may be as high as 65 to 85 MPa \sqrt{m} in the bcc Nb-Cr-Ti alloys, which have lower elevated-temperature oxidation limits (~700 °C) than the Laves-phase intermetallics (~1000 °C to 1200 °C). The fracture toughness levels in

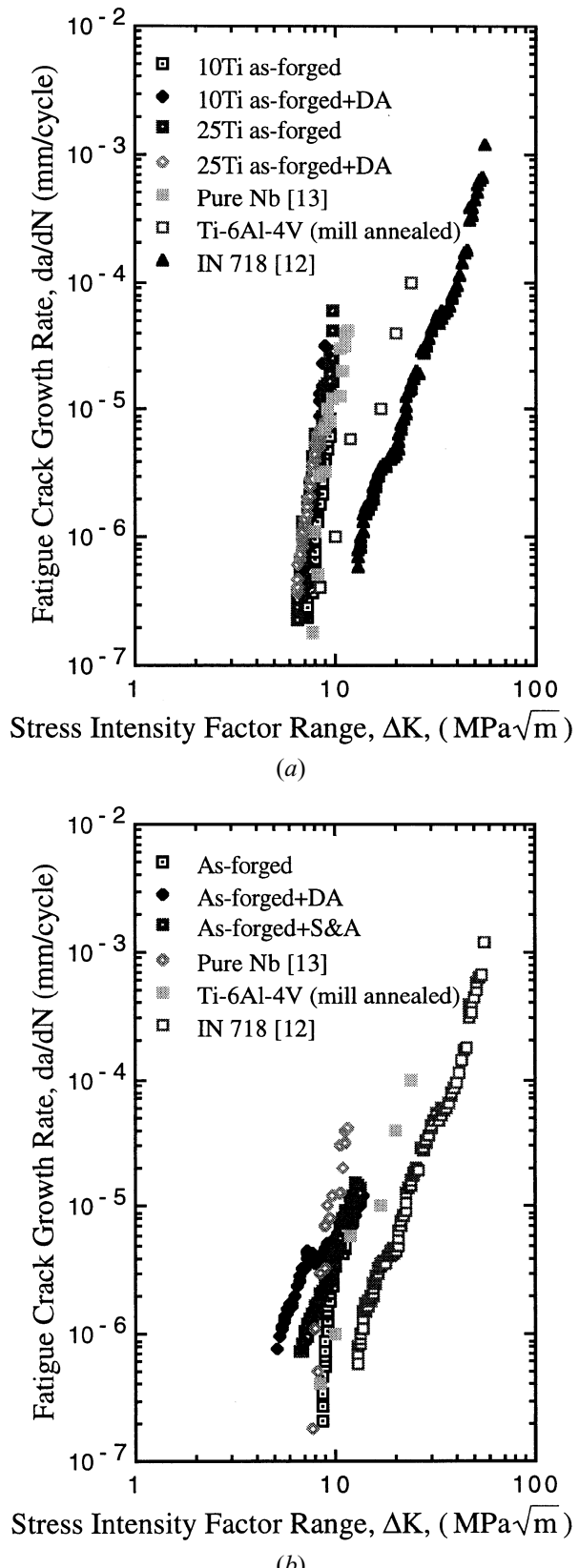
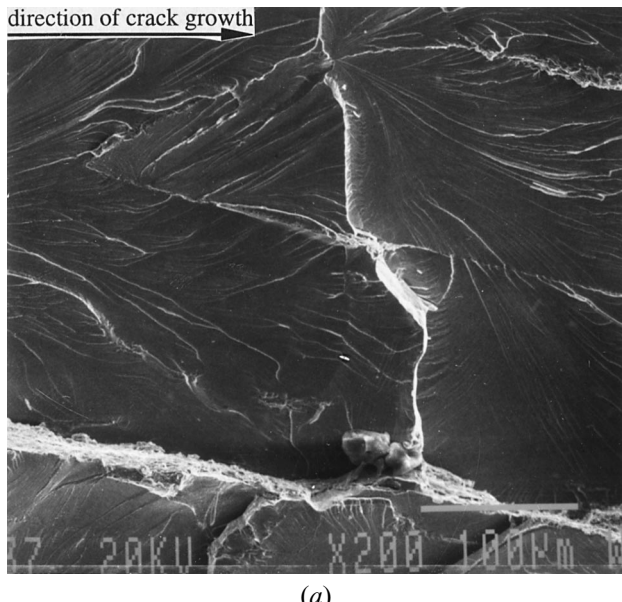


Fig. 8—Summary of fatigue growth rate data obtained for (a) forged 10Ti and 25Ti alloys and (b) forged Nb-15Al-40Ti.

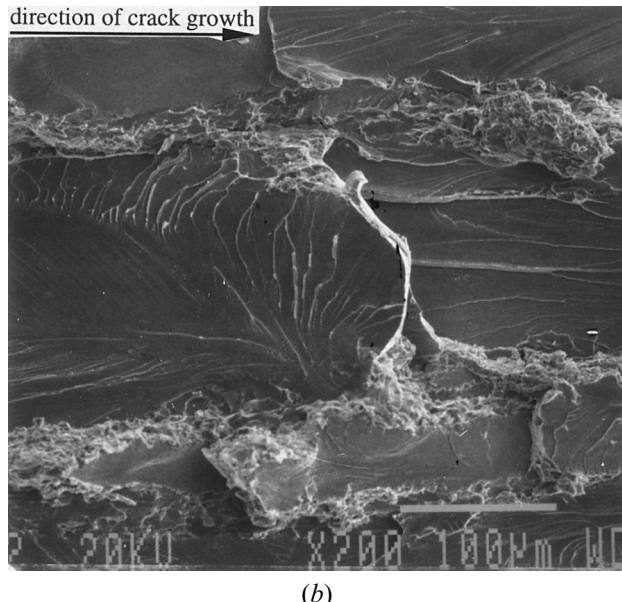
the Nb-Cr-Ti alloys also increase with increasing Ti contents up to 40 at. pct Ti, while those of the Laves-phase intermetallics decrease with Cr₂Nb content.^[4] Fracture

Table V. Summary of Paris Constants and Fatigue Thresholds in Nb-15Al-xTi Alloys

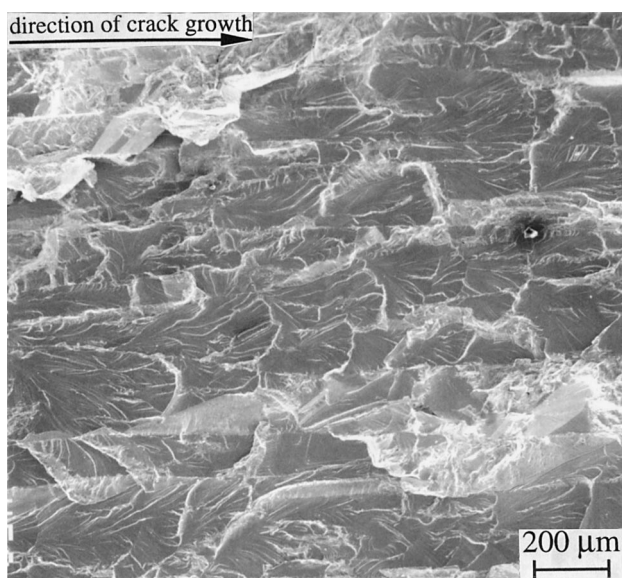
Material	Processes	Phase(s)	<i>m</i>	<i>A</i> (mm/cycle·(MPa/m) ^{-m})	ΔK_{th} (MPa \sqrt{m})
Nb-15Al-10Ti	as-forged	B2 + A15	13.7	4.3×10^{-19}	7.2
	as-forged + 750 °C/25 h	B2 + A15	19.6	7.0×10^{-24}	7.0
Nb-15Al-25Ti	as-forged	B2 + A15	10.4	1.5×10^{-15}	6.4
	as-forged + 750 °C/25 h	B2 + A15	8.5	7.6×10^{-14}	6.4
Nb-15Al-40Ti	as-forged	B2	9.7	5.0×10^{-16}	8.6
	as-forged + 750 °C/25 h	B2 + O	4.4	1.7×10^{-10}	6.7
	as-forged + 1150 °C/2 h + 750 °C/25 h	B2 + O	2.2	3.7×10^{-8}	5.1



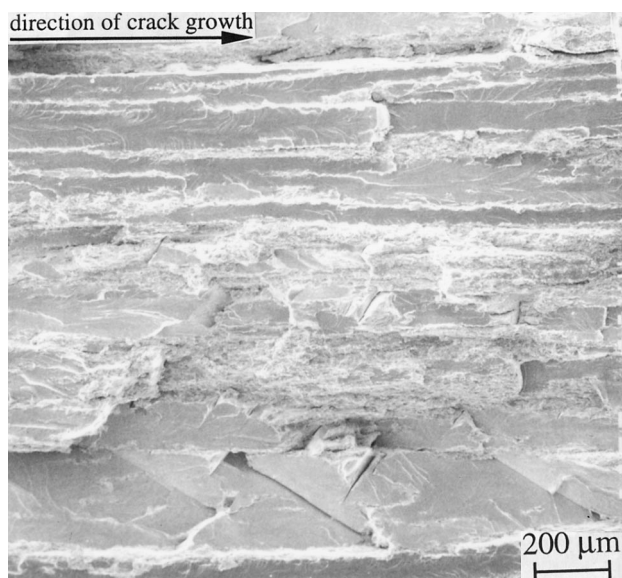
(a)



(b)



(c)

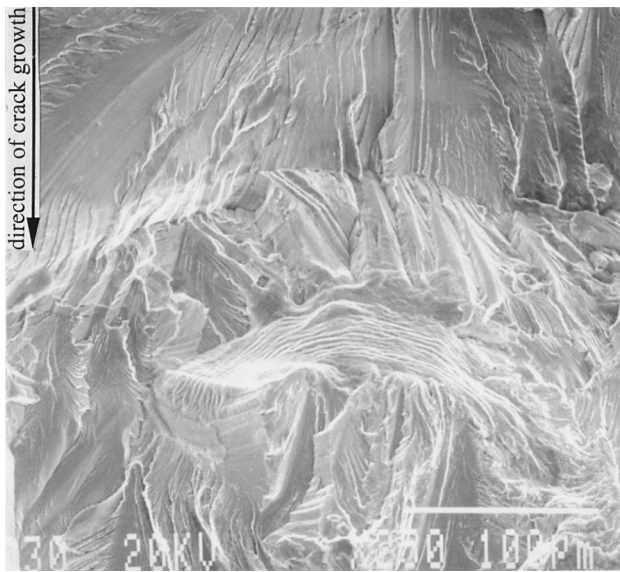


(d)

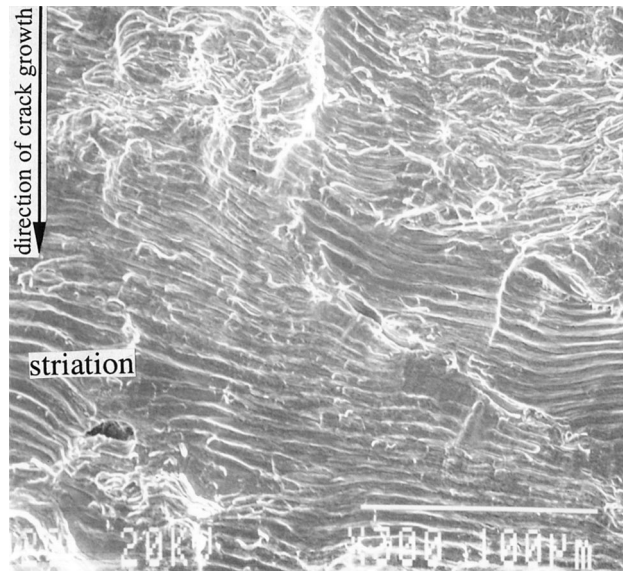
Fig. 9—Cyclic fatigue cleavage modes in forged 10Ti alloy: (a) as-forged and (b) as-forged + 750 °C/25 h; and forged 25Ti alloy: (c) as-forged and (d) as-forged + 750 °C/25 h.

toughness data have also been reported for Nb-Si and Nb-Cr-Ti-Hf-Si alloys.^[20] The niobium silicides have fracture toughness levels that are typically below ~ 35 MPa \sqrt{m} . The

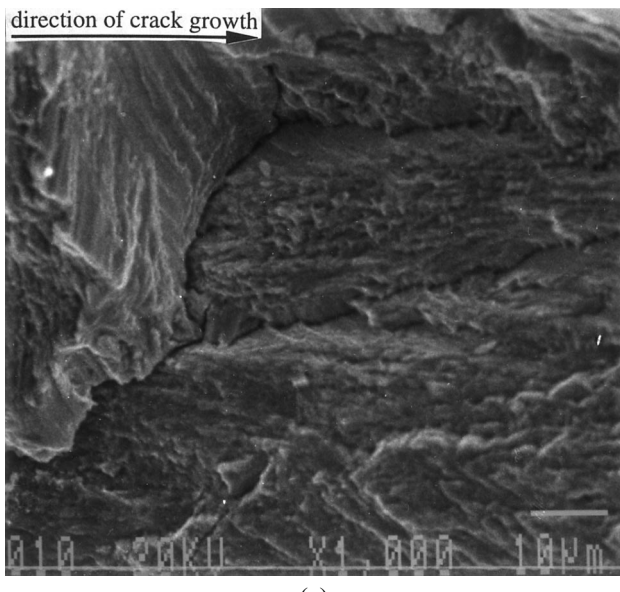
fracture toughness levels in these oxidation-resistant systems are due to the protective nature of complex mixed oxides^[20] that are formed on exposed surfaces of Nb-Si and



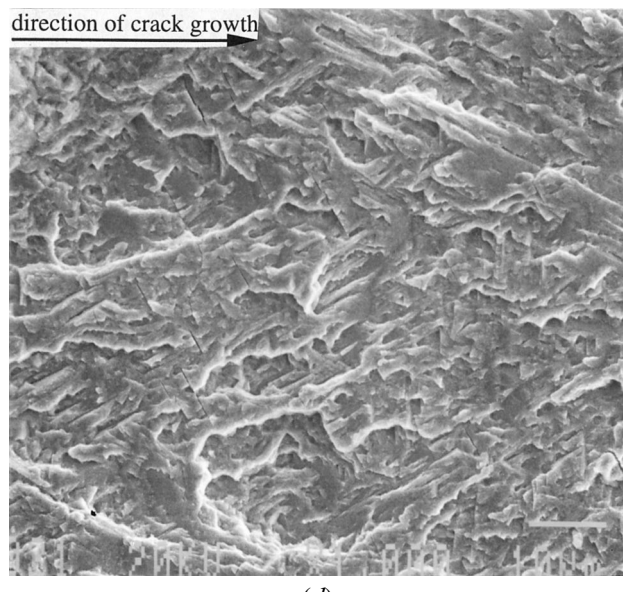
(a)



(b)



(c)



(d)

Fig. 10—Typical fatigue fracture mode in as-forged 40Ti: (a) low ΔK , (b) high ΔK , (c) secondary cracking in 40Ti (DA), and (d) relatively flat fracture surface of 40Ti (STA).

Nb-Cr-Ti-Hf-Si alloys. Typical fracture toughness levels for the toughest of the oxidation resistant Nb-Cr-Hf-Ti-Si alloys are ~ 20 to $26 \text{ MPa}\sqrt{\text{m}}$.^[22]

The fracture toughness levels of 40 to $110 \text{ MPa}\sqrt{\text{m}}$ reported in this article for the 40Ti alloy are, therefore, greater than those reported for other high-temperature niobium-based intermetallics. However, the toughness levels in the 40Ti alloy are comparable to those reported for the Nb-13Cr-37Ti alloys. The latter alloy has a density of $\sim 6.7 \text{ g/cm}^3$ ^[5] compared to the Nb-15Al-40Ti, which has a density of $\sim 6.1 \text{ g/cm}^3$.^[1] However, the other properties of the Nb-13Al-37Cr and Nb-15Al-40Ti alloys are generally comparable.

B. Fatigue Crack Growth

The fatigue crack growth resistance of the 40Ti alloy is also attractive. Unlike most intermetallics, the Paris exponents in this alloy are between 2.2 and 4.4. These relatively low (comparable to other intermetallics) Paris exponents are comparable to typical values for conventional structural metals and their alloys.^[17] Standard damage-tolerant design philosophies^[23] may, therefore, be used in the analysis and design of 40Ti structures and components. In contrast, most of the brittle intermetallic systems require initiation-based design concepts to prevent catastrophic failure due to fast fatigue crack growth rates,^[24] and short-crack phenomena.^[24] Such initiation-based methodologies may limit the structural benefits that can be achieved by the use of alternative high-temperature materials such as gamma-based titanium aluminides.^[24]

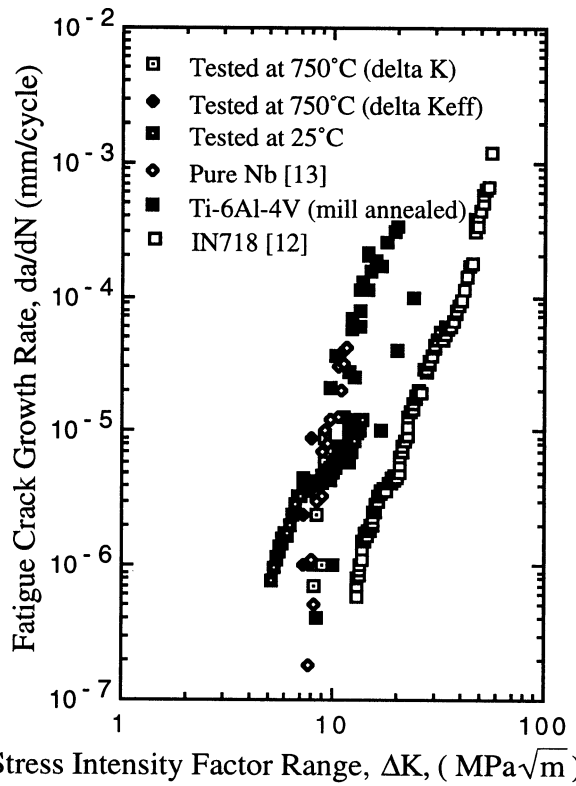


Fig. 11—Fatigue growth rates in as-forged + DA treated Nb-15Al-40Ti alloy at 25 °C and 750 °C.

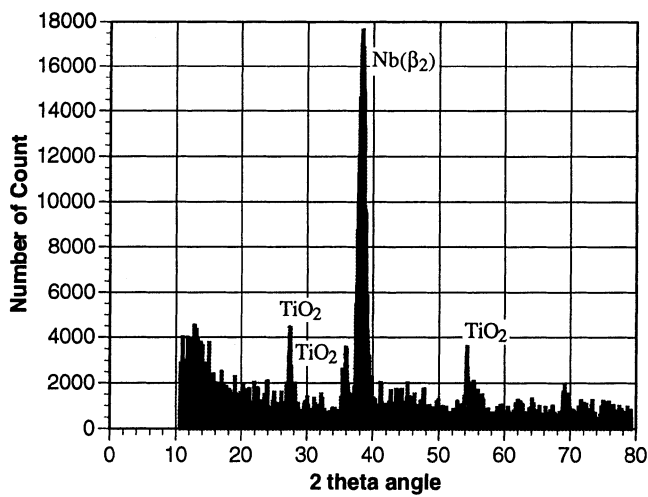


Fig. 12—X-Ray diffraction profile of fatigue crack growth specimen tested at 750 °C.

Finally, it is of interest to note that the slower fatigue crack growth rates at 750 °C (Figure 11) suggest that niobium aluminides may be used in the temperature regime between 25 °C and 750 °C. However, further work is needed to fully explore possible creep-fatigue crack interactions that can occur in this temperature regime. Detailed studies of the effects of environment on fatigue crack initiation and fatigue crack growth are also needed. Nevertheless, the attractive combinations of fracture toughness and fatigue crack growth resistance reported in this article sug-

gest that niobium aluminides may soon become strong candidates for intermediate-temperature structural applications.

VI. CONCLUSIONS

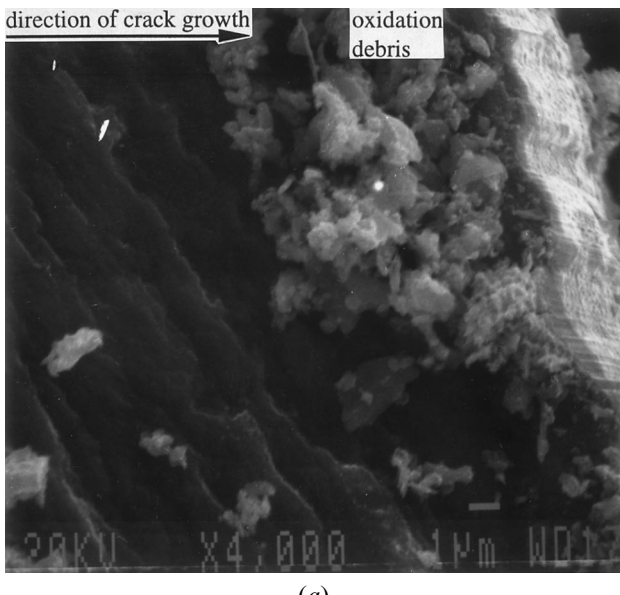
- Fracture in the brittle 10Ti and 25Ti alloys occurs by brittle cleavage fracture modes under monotonic loading. These alloys have relatively low fracture toughness levels of ~10 to 20 MPa√m at room temperature. In contrast, the tougher (40 to 100 MPa√m) 40Ti alloy exhibits ductile dimpled fracture modes (similar to those in metallic materials) in the as-forged and direct-aged conditions under monotonic loading. However, the 40Ti alloy fails by intergranular fracture after solid-solution treatment and annealing. Reasons for the transition to intergranular fracture in the STA condition are unknown at present.
- The fatigue crack growth rates in the 40Ti alloy are comparable to those in IN718, pure Nb, and Ti-6Al-4V at room temperature. Typical Paris exponents obtained for the 40Ti alloy (2.2 to 4.4) are also comparable to those in conventional structural alloys. However, the fatigue crack growth rates in the brittle 10Ti and 25Ti alloys are also much faster than those in the 40Ti alloy.
- Fatigue crack growth in the 40Ti alloy occurs by a “faceted” fracture mode in the near-threshold regime. Fatigue striations are observed in the mid- and high- ΔK regimes in the 40Ti alloy. Fatigue crack growth in the 10Ti and 25Ti alloys occurs by cyclic cleavage in the low-, mid-, and high- ΔK regimes.
- At 750 °C, thick oxide (TiO_2) scales (excess oxide thickness of ~5 μm) are formed on the fracture surfaces of the 40Ti alloy in the near-threshold regime. The slower near-threshold fatigue crack growth rates in this regime are due partly to the effects of oxide-induced closure, which occurs in the near-threshold regime when the crack opening displacements are comparable to the measured oxide thicknesses.

ACKNOWLEDGMENTS

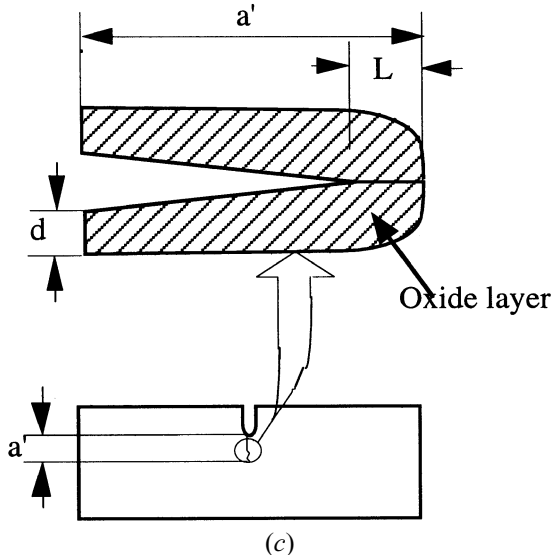
This research was supported by The Office of Naval Research (Grant No. N00014-94-1-0501). The authors are grateful to the Program Manager, Dr. George Yoder, for his encouragement and support. Appreciation is also extended to Mr. Andy Culbertson, The Naval Air Warfare Center, for providing additional financial support. The authors are also grateful to Professor Hamish Fraser, Dr. Mel Jackson, and Professor T.S. Srivatsan for useful discussions on niobium alloys and niobium-base intermetallics.

REFERENCES

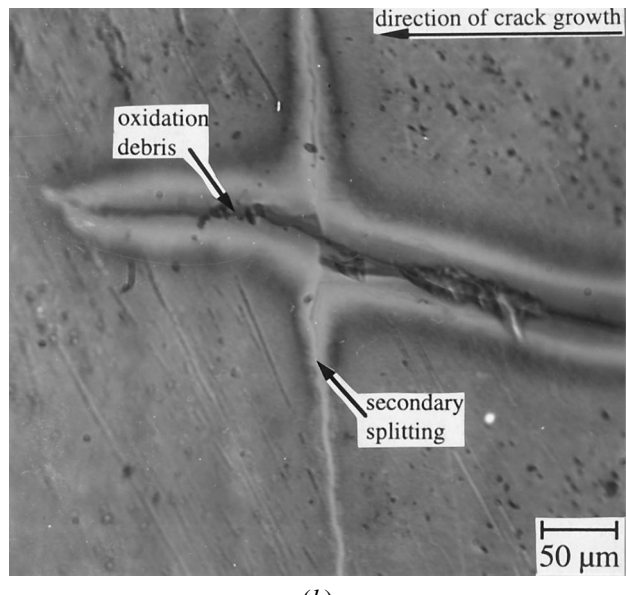
- D.H. Hou, J. Shyue, S.S. Yang, and H.L. Fraser: in *Alloy Modeling and Design*, G.M. Stocks and P.Z.A. Turch, eds., TMS, Warrendale, PA, 1994, pp. 291-98.
- J. DiPasquale, D. Gahutu, D. Konitzer, and W.O. Soboyejo: *High Temperature Ordered Intermetallic Materials—VI*, Materials Research Society Symposia Proceedings, J.A. Horton, I. Baker, S. Hanada, R.D. Noebe, and D.S. Schwartz, eds., Materials Research Society, Pittsburgh, PA, vol. 364. 1995, pp. 1347-52.
- T.S. Srivatsan, C. Daniels, S. Sriram, K.P. Dhana Singh, W.O. Soboyejo, and D. Konitzer: *Proc. Symp. on Fatigue and Fracture*



(a)



(c)



(b)

Fig. 13—Fatigue crack growth in the 40Ti alloy at 750 °C. (a) Oxidation debris and striations on the fracture surface. (b) Crack profile showing evidence of oxide layer and secondary splitting along intersecting grain boundary. (c) Schematic illustration of oxidation induced closure.

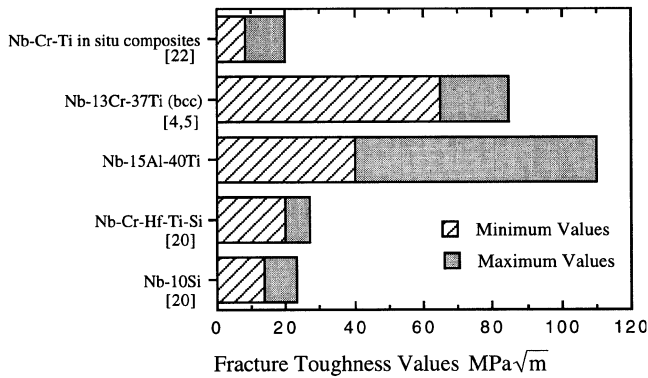


Fig. 14—Comparison of fracture toughness values.

- of Ordered Intermetallics II, W.O. Soboyejo, T.S. Srivatsan, and R.O. Ritchie, eds., TMS, Warrendale, PA, 1995, pp. 287-308.
4. D.L. Davidson, K.S. Chan, and D.L. Anton: *Metall. Mater. Trans. A*, 1996, vol. 27A, pp. 3007-18.
 5. D.L. Davidson, K.S. Chan, and D.L. Anton: *Metall. Mater. Trans. A*, 1997, vol. 28A, pp. 1797-1808.

6. K.S. Chan: *Metall. Mater. Trans. A*, 1996, vol. 27A, pp. 2518-31.
7. J. Shyue, D.-H. Hou, S.C. Johnson, M. Aindow, and H.L. Fraser: *Mater. Res. Soc. Proc.*, 1993, vol. 288, pp. 243-50.
8. *Binary Phase Diagrams*, T.B. Massalski, ed., ASM, Metals Park, OH, 1986.
9. S. Das, T.J. Jewett, and J.H. Perepezko: *Structural Intermetallics: Proc. 1st Int. Symp. on Structural Intermetallics*, R. Darolia, J.J. Lewandowski, C.T. Liu, P.L. Martin, D.B. Miracle, and M.V. Nathal, eds., TMS, Warrendale, PA, 1993, p. 35.
10. H.L. Fraser: Research Report, Office of Naval Research, Arlington, VA, 1996.
11. S. Suresh and J.R. Brockenbrough: *Acta Metall. Mater.*, 1988, vol. 36, pp. 1444-70.
12. "Metals Tests Methods and Analytical Procedures," *Annual Book of ASTM Standards*, ASTM, Philadelphia PA, 1993, Sect. 3.
13. S. Johnson: Ph.D. Thesis, The Ohio State University, Columbus, OH, 1997.
14. S. Dubey, A.B.O. Soboyejo, and W.O. Soboyejo: *Acta Metall. Mater.*, 1997, vol. 45, pp. 2777-87.
15. C. Mercer and W.O. Soboyejo: in *Superalloy 718, 625, 706 and Various Derivatives*, E.A. Loria, ed., TMS, Warrendale, PA, 1997, pp. 577-86.
16. N. Polvanich and K. Salama: *ASTM STP 962*, L. Raymond, ed., ASTM, Philadelphia, PA, 1987, pp. 417-27.

17. S. Suresh: *Fatigue of Materials*, Cambridge University Press, Cambridge, United Kingdom, 1991.
18. S. Suresh and R.O. Ritchie: in *Fatigue Crack Growth Threshold Concepts*, D.L. Davidson and S. Suresh, eds., AIME, Warrendale, PA, 1984, pp. 227-61.
19. D. Farkas: unpublished research, Virginia Polytechnic Institute & State University, Blacksburg, VA, 1997.
20. C. Mercer and W.O. Soboyejo: *Acta Metall. Mater.*, 1997, vol. 45, pp. 961-71.
21. W.O. Soboyejo, F. Ye, L.-C. Chen, N. Bahtishi, D.S. Schwartz, and R.J. Lederich: *Acta Metall. Mater.*, 1996, vol. 44, pp. 2027-41.
22. B.P. Bewlay, J.J. Lewandowski, and M.R. Jackson: *J. Met.*, 1997, Aug., pp. 44-67.
23. J.M. Larsen, B.D. Worth, C.G. Annis, Jr, and F.K. Haake: *Int. J. Fract.*, 1996, vol. 80, pp. 237-55.
24. J.M. Larsen, B.D. Worth, S.J. Balsone, A.H. Rosenberger, and J.W. Jones: *Fatigue' 96*, Elsevier Science Ltd., Oxford, United Kingdom, 1996, vol. III, pp. 1719-30.